JOURNAL OF GEOPHYSICAL RESEARCH, VOL. 104, NO. B12, PAGES 28,723-28,739, DECEMBER 10, 1999

Cause of continuous oscillations of the Earth

Toshiro Tanimoto and Junho Um
Institute of Crustal Studies and Department of Geological Sciences
University of California, Santa Barbara

Abstract. Spheroidal fundamental mode oscillations of the Earth for frequencies between 2 and 7 mHz (millihertz) are observed even on seismically quiet days. Two hypotheses of the cause of these oscillations are investigated: the cumulative effect of small earthquakes and atmospheric pressure variations. The cumulative effect of earthquakes, assuming that earthquakes follow the Gutenberg-Richter law, is shown to be 1-2 orders of magnitude too small. The observed amplitudes of modes require an equivalent earthquake of magnitude 6.0 everyday, which cannot be achieved by summing up contributions from small earthquakes. The hypothesis of atmospheric excitation is favored because of the discovery of seasonal variations in stacked modal amplitudes for spheroidal modes between ${}_0S_{20}$ and ${}_0S_{40}$. It is also evaluated by comparing observed modal amplitudes with theoretical amplitudes, derived from a stochastic normal mode theory. The source of excitation is atmospheric pressure variations, which indicate turbulent motion of the atmosphere for the frequency range of interest and are estimated by barometer data. The observed modal amplitudes can be matched by the stochastic normal mode theory, indicating that atmospheric pressure variation is large enough to excite solid Earth normal modes up to the observed amplitudes. Therefore two lines of evidence, detection of seasonal variations and approximate match of overall modal amplitudes, support the hypothesis that the continuous background oscillations are excited by atmospheric pressure variations.

1. Introduction

It is well known that the Earth oscillates at characteristic resonant frequencies after large earthquakes. But it has been shown recently, much to our surprise, that the Earth may be oscillating continuously, regardless of the occurrence of large earthquakes. Evidence was pointed out by various groups based on different data; *Nawa et al.* [1998] have shown evidence from a superconducting gravimeter in Antarctica, *Suda et al.* [1998] from the International Deployment of Accelerometers (IDA) gravimeter data, *Tanimoto et al.* [1998] from the IDA gravimeter data [*Agnew et al.*, 1986] and the Geoscope broadband seismic data [*Roult and Montagner*, 1994], and *Kobayashi and Nishida* [1998] from the Incorporated Research Institutions for Seismology (IRIS), Global Seismic Network (GSN) broadband seismic data.

While the initial claim by *Nawa et al.* [1998] was made for superconducting gravimeter data for a frequency range between 0.3 mHz and 5 mHz, signals from a slightly different frequency range, between 2 and 7 mHz, can be confirmed by conventional broadband seismometer records. Plates 1a and 1b show Fourier spectral amplitudes at two Geoscope stations, KIP (Kipapa) and CAN (Canberra). Spectral amplitudes of acceleration from each day over 3-4 years are plotted vertically with three colors; blue, yellow, and red denote amplitudes of acceleration less than 0.4 nGal, between 0.4 and 2 nGal, and above 2 nGal, respectively. Fundamental spheroidal mode eigenfrequencies of the Preliminary Reference Earth model (PREM) [*Dziewonski and Anderson*, 1981], are shown by arrows on the lefthand side, and their range is from ${}_0S_{22}$ to ${}_0S_{32}$. In both plates, horizontal (yellow) stripes are observed almost continuously at the eigenfrequencies of fundamental spheroidal modes. While occasional high seismic activity produces red and yellow regions and tends to bury the yellow stripes due to background oscillations, the yellow horizontal stripes can be identified through the years and suggests that these modes exist irrespective of (large) earthquake occurrence.

The aim of this paper is to examine the cause of these oscillations by focusing on two hypotheses. The first hypothesis is excitation of these modes by cumulative effects of small earthquakes. The Earth, being an active planet, has many small earthquakes that are not reported in standard earthquake catalogues. It thus seems natural to consider cumulative effects of small earthquakes for the excitation of normal modes. We will demonstrate, however, that such effects are too small and are also incompatible with some aspects of the observations. *Suda et al.* [1998], *Tanimoto et al.* [1998], and *Kobayashi and Nishida* [1998] pointed this out re-

Paper number 1999JB900252.
0148-0227/99/1999JB900252$09.00

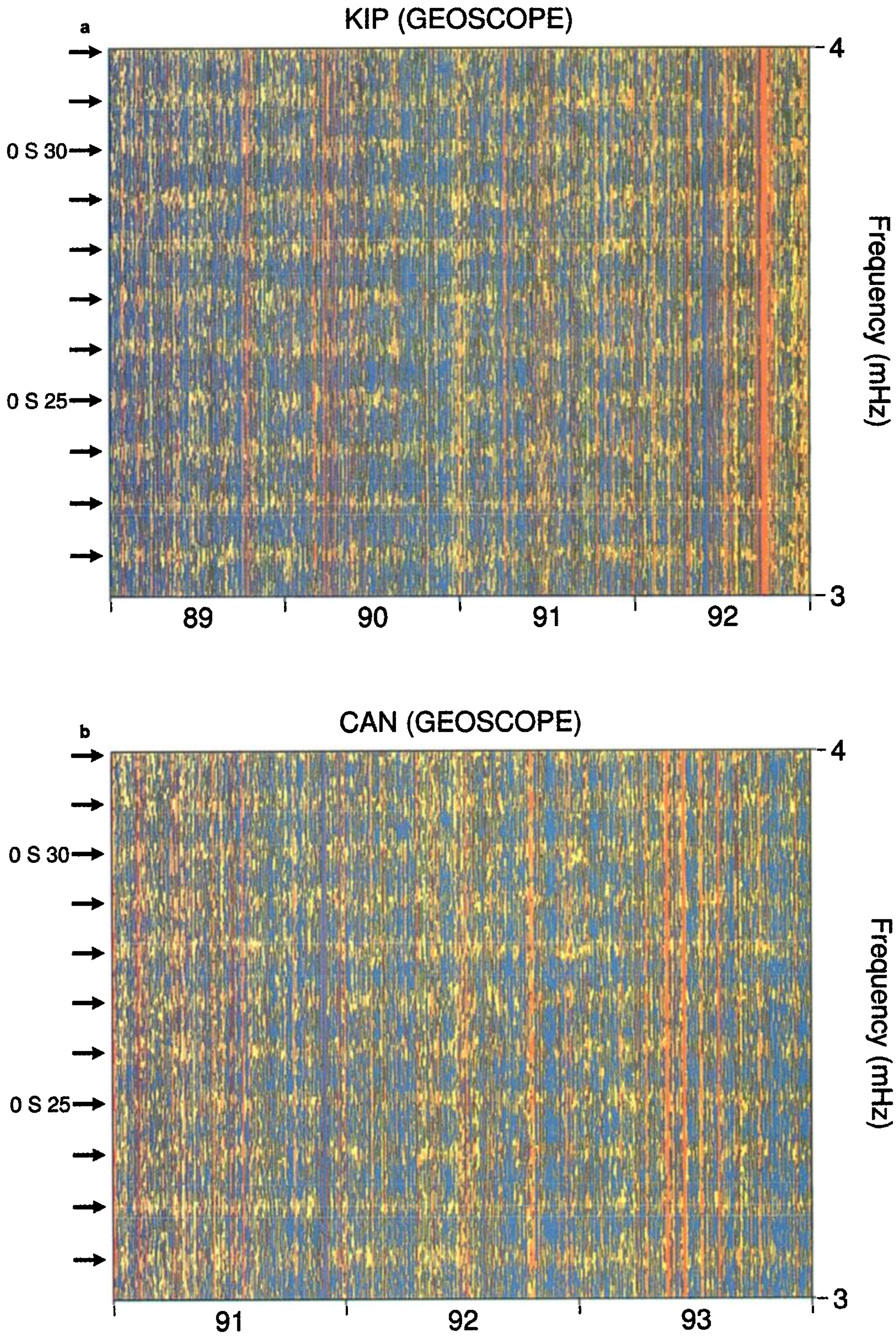

Plate 1. (a) Spectral amplitude at KIP for frequencies between 3 mHz and 4 mHz during the period between 1989 and 1992. For each day, there is a vertical line. Three different colors, blue, yellow, and red, denote three different levels of amplitudes, and indicate amplitudes less than 0.4 nGal, between 0.4 and 2 nGal, and larger than 2 nGal, respectively. On days of large earthquakes and their subsequent few days, vertical red lines appear. The arrows on the left-hand side of the figure indicate the eigenfrequencies of fundamental spheroidal modes of the Preliminary reference eEarth model (PREM). Angular degrees of modes are from 22 to 32. Yellow horizontal stripes are seen at the eigenfrequencies of modes and suggest that they are continuously excited modes. (b) Same as Plate 1a, except that this is for CAN for the period between 1991 and 1993.

cently. We add two more arguments against this hypothesis to strengthen this conclusion and, at the same time, to clarify the underlying assumptions in the arguments.

The second hypothesis is the excitation by atmospheric pressure variations; the atmosphere applies pressure variations everywhere on the surface of the Earth, continuously in time. While such effects may be small locally, integrated effects for the entire globe may excite normal modes. This hypothesis is favored in this paper, particularly because average modal amplitudes for fundamental modes ${}_0S_{20}$-${}_0S_{40}$ show seasonal variations; high amplitudes are seen in June-August and December-February, and low amplitudes are seen in March-May and September-November. Generally speaking, amplitudes are high in summer and winter when either the north pole or the south pole is pointing toward the Sun and are low in spring and autumn. It would be hard to imagine that sources in the solid Earth such as earthquakes could create such seasonal patterns.

Quantitative evaluation of the atmospheric hypothesis is also pursued in this paper, which requires a version of normal mode theory that is different from previous terrestrial normal mode analyses [e.g., *Gilbert*, 1971; *Saito*, 1967; *Dahlen*, 1968]. This is due to the stochastic nature of atmospheric pressure variations for frequencies above 0.5 mHz. Since force by atmospheric turbulence is stochastic, a stochastic excitation theory of the Earth's oscillations, developed by *Tanimoto* [1999], is applied. Input for the force term, that is, the pressure variations at the surface, is derived from barometer data for this purpose. We collect barometer data from U.S. Geological Survey (USGS) and Terrascope networks, which show similar behavior among various stations for average pressure and their variations. It is shown that a good quantitative match between the observed modal amplitudes and theory can be achieved with the use of estimated pressure variations.

In developing the stochastic normal mode theory, we take a view that the atmosphere is separate from the solid Earth. We regard the atmosphere as the external source that applies the (surface) force on the solid Earth. This approach is different from the coupled mode approach developed by *Watada* [1995] and *Lognonné et al.* [1998] for the analysis of volcanic explosion data, which views the media as a system consisting of the atmosphere and the solid Earth. This difference is not important for our conclusions, however, because we are primarily interested in fundamental mode oscillations of the Earth. Fundamental modes must have oscillating counterparts in the atmosphere, but atmospheric contributions to the modal mass (defined later) are much smaller than contributions by the solid Earth. Since the modal mass determines the level of excitation, the two different views should yield basically the same answer.

In section 2 we will discuss seismic (spectral amplitude) data, which are the basic data to be explained by the theory, and barometer data, which will be used to estimate the source of excitation for the atmospheric excitation hypothesis. We will then discuss, in section 3, the cumulative effects of earthquakes and the reasons why we do not consider it to be a viable hypothesis. In section 4 we show evidence of seasonal variations in stacked (averaged) modal amplitude data. In section 5 we evaluate the excitation hypothesis quantitatively by atmospheric pressure variations. Discussions will follow in section 6. In this paper we will focus on these two mechanisms and will not discuss the effect of slow or silent earthquakes [*Beroza and Jordan*, 1990]. We do not question the existence of such earthquakes, but they would not likely create continuous oscillations with seasonal variations.

2. Data

We first discuss modal amplitude measurements for Geoscope and IRIS GSN data, which constitute the basic data set in this study. Acceleration amplitudes of spheroidal modes between 3 mHz and 7 mHz are estimated from this analysis. We then describe barometer data from USGS and Terrascope which will be used to estimate pressure variations on the surface. A model of pressure variation is constructed from this analysis and will be used for a theoretical estimate of normal mode amplitudes in the next section.

2.1. Modal Amplitudes

The basic data to be fit by theory are modal amplitudes measured at six broadband seismic stations; they consist of two Geoscope stations (KIP and CAN), and four IRIS GSN stations (PAS, HRV, PFO, and SUR). Locations of stations are given in the top six rows of Table 1. We measure modal amplitudes following the basic procedure described by *Tanimoto et al.* [1998]. The main idea is to exclude earthquake effects as much as possible from the data and then measure the average spectra from the remaining time periods. The procedure for excluding earthquake effects consists of a two-step process: (1) use of earthquake catalogues to remove the days of large earthquakes and the subsequent 3-5 days, depending on the size of the earthquakes, and (2) visual examination in order to remove data that are affected by local (small) earthquakes. We ensure that no hint of earthquakes is found in the data through this process. We then compute the Fourier spectral amplitudes for each of the 1-day length data to generate the average spectral amplitude. Technically, we perform the following analysis; for each seismically quiet day, we compute

$$U(\omega) = \frac{4}{T}\int_0^T w(t)u(t)e^{-i\omega t}dt, \qquad (1)$$

where $w(t)$ is the Hanning window, $u(t)$ is the 1-day time series, and ω is the angular frequency. The coefficient $4/T$ exists so that if $u(t)$ has a sinusoidal form of $A\cos(\omega t)$ or $A\sin(\omega t)$, the spectral amplitudes become equal to $A = |U(\omega)|$ for the frequency range of interest. We then remove instrument response effects from $U(\omega)$ by division, convert it to units of acceleration, and then

Table 1. Geographic Location of Stations

Station	Latitude, (deg N)	Longitude, (deg E)	Altitude, (m)	Analyzed Instrument
CAN	-35.321	148.999	651	STS-1
KIP	21.423	-158.015	70	STS-1
HRV	42.506	-71.558	180	STS-1
PAS	34.148	-118.172	250	STS-1
PFO	33.609	-116.455	1250	STS-1 and Barometer
SUR	-32.380	20.818	1770	STS-1
INU	35.350	137.029	132	STS-1
GSC	35.303	-116.808	990	STS-1 and Barometer
ESK	55.317	-3.205	242	STS-1
BDFB	-15.64	-48.01	1195	Barometer
BOSA	-28.61	25.55	1280	Barometer
DBIC	6.67	-4.86	125	Barometer
LBTB	-25.02	25.60	1128	Barometer
PLCA	-40.73	-70.55	1050	Barometer

stack the records. Examples from two IRIS stations, PAS and HRV, are shown in Figure 1.

There are two aspects to be noted in these stacked spectra; the first is the low frequency, with a rising trend toward lower frequencies below 3 mHz. The other is a sequence of fundamental mode peaks between 3 and 7 mHz, clearly emerging above the background trend exactly at the eigenfrequencies of normal modes.

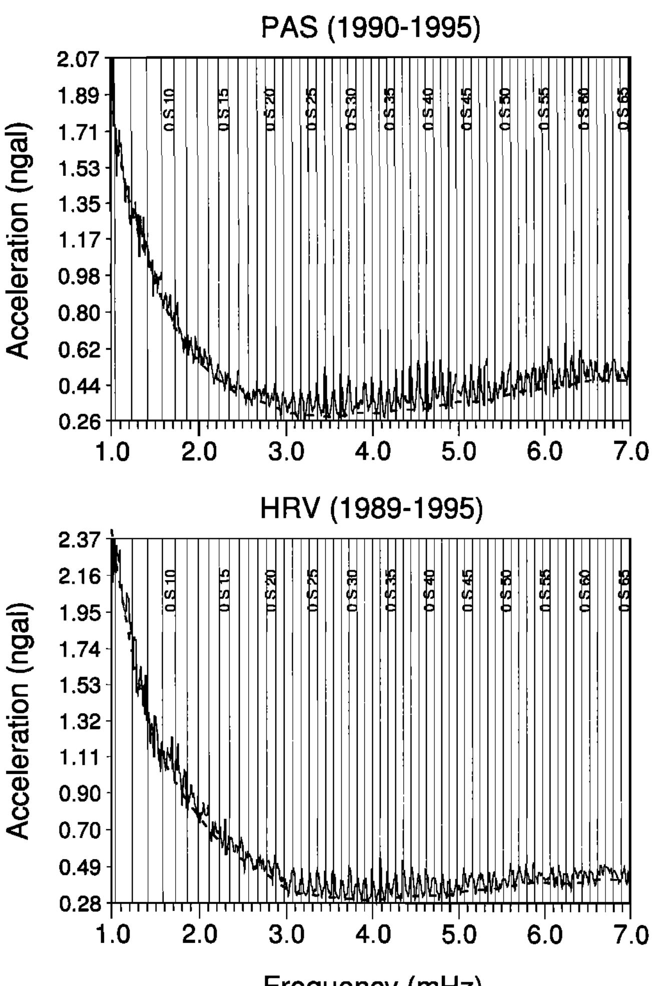

Figure 1. Stacked spectral amplitudes from seismically quiet days at PAS and HRV. Background trends, shown in the figure by dashed lines, are removed when modal amplitudes are estimated. Modal amplitudes are measured for all spheroidal fundamental modes between 3 mHz and 7 mHz.

The rising background noise level is almost certainly caused by gravitational attraction of temporarily changing atmospheric mass near a station. This mechanism predicts good correlation between a seismometer and a barometer which are colocated at the same station. Available data indicate some correlation, and *Zürn and Widmer* [1995] took advantage of this fact to reduce long period noise from seismic data. Note that before *Zürn and Widmer* [1995], correlation was observed mainly in the tidal frequency band, typically for frequencies less than 0.1 mHz [e.g., *Warburton and Goodkind*, 1977, 1978; *Müller and Zürn*, 1983; *Crossley et al.*, 1995], but existence of such correlations in the millihertz range had not been demonstrated. Terrascope provides a unique array of such colocated barometers and broadband seismometers, from which we also confirmed existence of such correlations. *Tanimoto* [1999] discussed a different view, which claimed that surface pressure fluctuation due to turbulent atmosphere contributes to this rising trend. In view of the good correlation between barometers and seismometers, this view should be rejected. However, the theoretical formulation for the stochastic excitation of normal modes of *Tanimoto* [1999] may be of some value and is actually used in a later section.

In the analysis of modal amplitude data, we will proceed with the assumption that background noise and modal signals are independent. Some questions may be raised on this point. Our analysis is mainly based on our belief that the background noise above 3 mHz is not caused by the atmosphere, while signals (modal peaks) are caused by the atmospheric pressure variations. Noise in ground acceleration measurements, below 3 mHz, is clearly controlled by the atmosphere and has an inverse frequency trend ($1/f$), similar to the trend in barometer spectra. Noise above 3 mHz, however, changes its character and becomes flat up to about 50 mHz (with a possible broad small peak in between). On the other hand, barometer spectra show the continued inverse frequency trend ($1/f$) for frequencies much above 3 mHz, which we confirmed at least up to 10 mHz. Clearly, this change in the noise trend in ground acceleration suggests a change in the controlling mechanism of noise at about 3 mHz, that is, something other than the atmosphere causes ground motion noise above 3 mHz; if the modes were excited by atmospheric pressure variations, they should naturally be independent from the background noise, and the following analysis would be justified. This view is not, obviously, model independent and may require further scrutiny in the future.

Under the assumption of independence, we first derive the smooth noise level as shown in Figure 1 by the dashed lines. Let us denote it by $U_N(\omega)$ (dashed line) and the stacked spectral amplitude by $U(\omega)$. Modal amplitudes are then obtained by $\sqrt{U^2(\omega) - U_N^2(\omega)}$ at each eigenfrequency of modes, assuming the two signals are independent phenomena. Measured modal amplitudes by this procedure are given in Table 1 and are also plotted in Figure 8 with theoretical curves.

2.2. Barometer Data

We analyze barometer data in order to construct a model of pressure variations as a function of frequency. This model is used for evaluation of atmospheric effects. We examined three Terrascope stations (ISA, GSC, and PFO) and five USGS stations (BDFB, BOSA, DBIC, LBTB, and PLCA), all of which have high-frequency barometer data, sampled at every second. Their locations are given in Table 1 and are from various parts of the world.

Figure 2a shows the spectral amplitudes at GSC for frequencies between 0.1 mHz and 10 mHz. The first 20 days of 1994 were analyzed to generate this spectrum. Selection of other time intervals generates similar amplitude behavior. Above a frequency of about 0.5 mHz, the spectral amplitudes typically show a $1/f$ decreasing trend, a consistent feature at all other stations. They also show very rapidly changing amplitude variations above frequency 0.5 mHz, suggesting very complex behaviors of atmospheric motion. We speculate that this is related to turbulence in the atmospheric boundary layer, which should have $1/f$ pressure variations on the average, if it follows the Kolmogorov (Monin-Obukhov) scaling law [e.g., *Tennekes and Lumley*, 1972, *Landau and Lifshitz*, 1987]. Similar behavior of wind velocity data is often reported in the meteorological literature [e.g., *Kaimal and Finnigan*, 1994; *Garratt*, 1992; *Panofsky and Dutton*, 1984]. As expected for spectra related to turbulence, correlation analyses among close stations such as GSC, ISA and PFO show very little correlation (Figure 2b), and yet they all seem to have approximately similar spectral amplitude behavior on the average. In other words, phase shows very little coherence, but averaged amplitude data show systematic

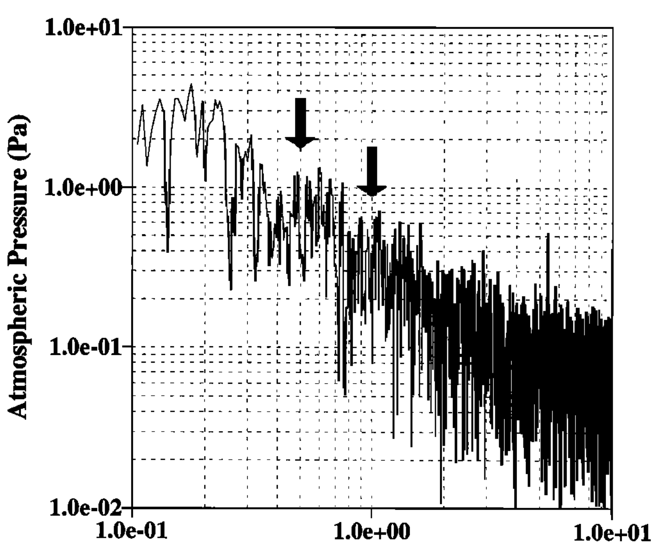

Figure 2a. Fourier spectral amplitude of barometer data at GSC (Terrascope) for the first 20 days of 1994. Two arrows are at 0.5 mHz and 1 mHz; the energy-containing eddies must exist near these frequencies and turbulent energy cascades toward higher frequencies. The $1/f$ trend is consistent with the Kolmogorov scaling of turbulence.

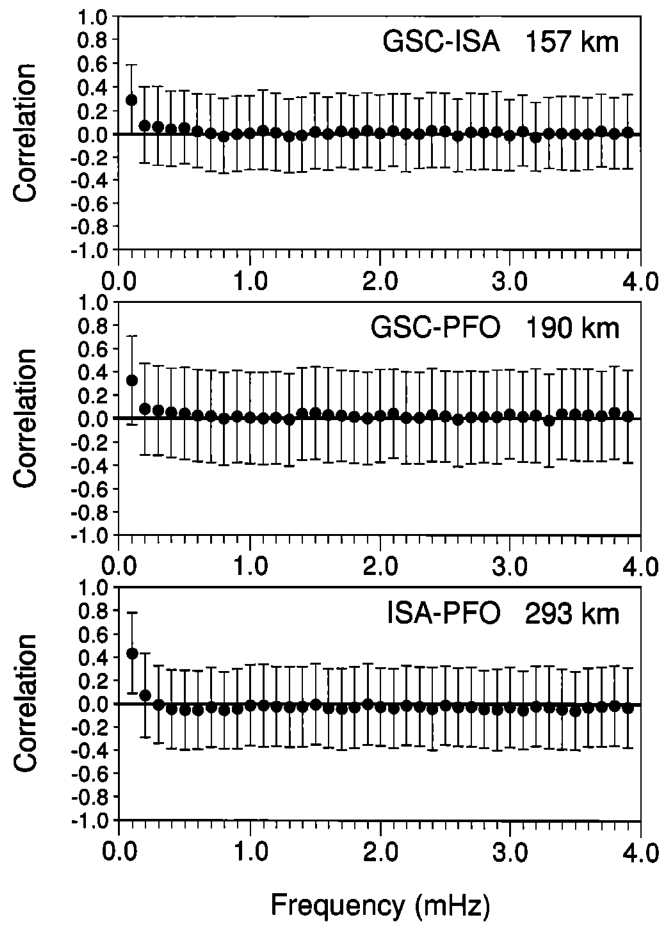

Figure 2b. Correlations among nearby barometer stations (Terrascope) for various narrow (±0.1 mHz) frequency bands. Station distances vary from 157 km to 297 km. There exist virtually no correlations for frequencies above 0.1 mHz. Surface pressure variation is a stochastic source with short correlation distance.

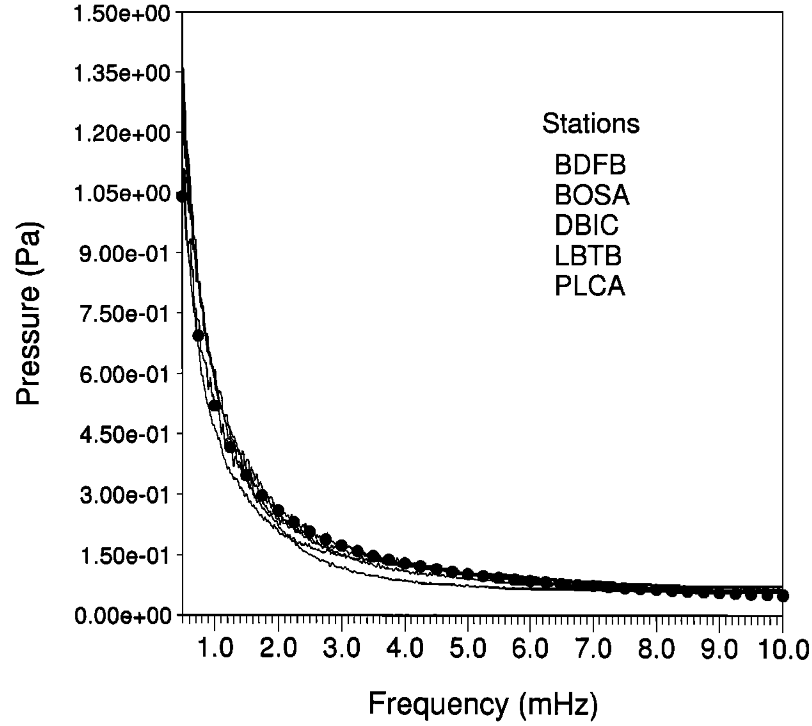

Figure 3a. Average pressure spectra from five USGS stations are shown by solid lines, and the average model, which we constructed with fixed $1/f$ trend, is shown by circles. The $1/f$ trend is predicted by Kolmogorov scaling and fits the data well, although the data deviate from it slightly.

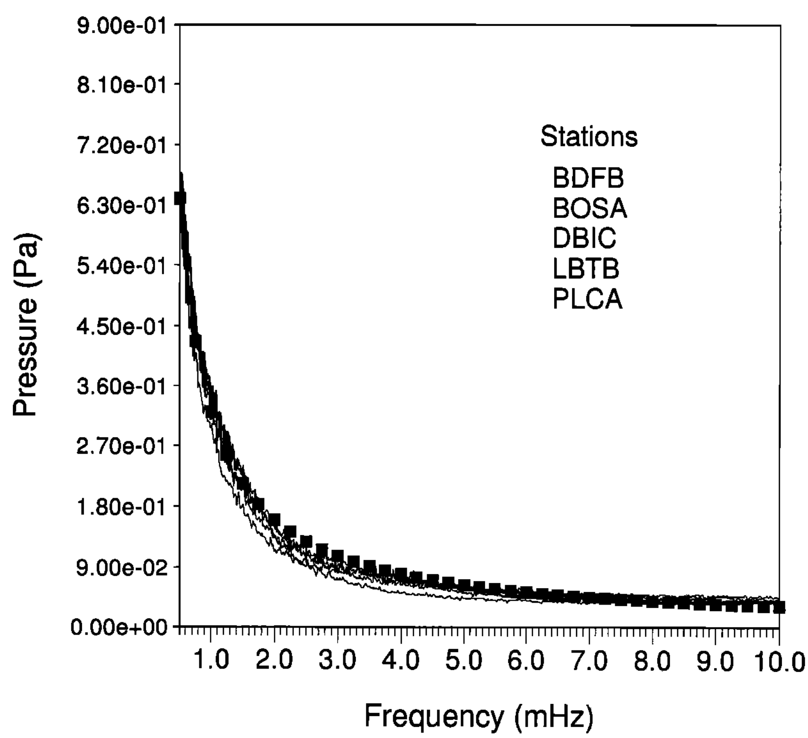

Figure 3b. Average pressure variations from five USGS stations. They describe standard error about the average pressure given in Figure 3a. The model is shown by squares. As predicted by Kolmogorov scaling, pressure variations also have $1/f$ trend.

$1/f$ behavior at all stations, which is consistent with the picture of fully developed turbulence.

These observations suggest that energy-containing eddies exist near 1 mHz and turbulent energy cascades toward higher frequencies. However, the precise frequency of the energy-containing eddies is hard to determine observationally. As we discuss in later sections, this will bring in some uncertainties for theoretical estimation of modal amplitudes.

Figure 3a shows average spectral amplitudes of barometer data for five USGS stations. We computed the Fourier spectra for each day for 2-3 years worth of data and took an average of all the data for each station. It is clear that pressure shows a $1/f$ trend as the scaling law implies. The best fit $1/f$ trend is shown by circles and its formula is given by $P(f) = 0.52/f$, where P is in Pascals and f is in millihertz.

Pressure variations about the average pressure (estimated above) are substantial as Figure 2a indicates. They are equivalent to the standard errors of pressure about the mean given by the above formula. They are shown in Figure 3b, which also has a $1/f$ trend, as the Kolmogorov scaling predicts. The best fit to these data is shown by squares in the figure and its formula is given by $P(f) = 0.32/f$ with the same units. These pressure variations are used for the source of atmospheric excitation in the theoretical modal amplitude estimate.

In obtaining average pressure and pressure variation models, given by the two formulas above, the data were corrected for the station altitudes. Altitude correction amounts to multiplying the spectral amplitudes by $\exp(z/H_s)$, where z is the altitude of the station and H_s is the scale height of the atmosphere and follows from the following model: We assume a simple static atmospheric model which has the density distribution given by

$$\rho = \rho_0 e^{-z/H_s}, \tag{2}$$

where ρ_0 is the surface density and the surface is $z = 0$. Pressure at altitude z is obtained by the integration

$$P(z) = \int_z^\infty \rho g dz = \rho_0 g H_s e^{-z/H_s}. \tag{3}$$

The ratio of pressure at altitude z and at altitude 0 is given by e^{-z/H_s}. Correction by this term is typically 0-15(station altitudes are about 0-1500 m) and shrinks the scatter in data. The data in Figures 3a and 3b (solid lines) are all referenced to $z = 0$ by this procedure.

3. Small-Earthquake Effects

Since the Earth is a tectonically active planet, it may seem natural to consider cumulative effects of small earthquakes to be the cause of these continuous oscillations. An order of magnitude argument against this hypothesis was presented by *Tanimoto et al.*, [1998] and *Kobayashi and Nishida* [1998]. *Suda et al.* [1998] also presented some arguments against it based on the calculations for all Harvard moment tensor solutions. We add two more arguments against this hypothesis in this section; the first set of evidence in section 3.1 does not seem to have been pointed out by others. The second argument overlaps, to some extent, with the arguments already presented by others but is presented here for clarity. The main conclusion is that as long as the Gutenberg-Richter law for magnitude-frequency relation holds for small earthquakes, with a b value of about 1, the cumulative effect of small earthquakes cannot be the cause of these oscillations.

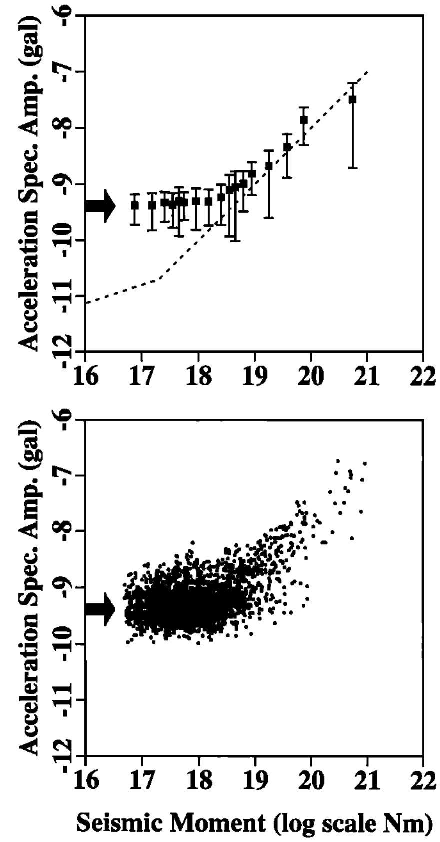

Figure 4a. Amplitudes of ${}_0S_{26}$ at KIP are plotted against the cumulative moment of each day. Raw data are shown at bottom. The top panel shows the median and variance (L1 norm) estimated from the raw data. Data with earthquakes larger than 10^{18} Nm show linear trend; this is because low-frequency amplitudes are proportional to moment. This linearity is approximated by the dashed line. Amplitudes of this mode become flat for earthquakes below about 10^{18} Nm. This continues to seismically quiet days, whose amplitudes are indicated by the arrows.

3.1. Plot of A_{26} Versus Moment

The first argument is purely observational. Figures 4a and 4b show the plot of measured acceleration amplitude of the mode ${}_0S_{26}$ (hereafter A_{26}) against the (cumulative) moment of each day. The Harvard moment tensor catalogue [*Dziewonski and Woodhouse*, 1983] was used for moment calculations for each day. Raw data

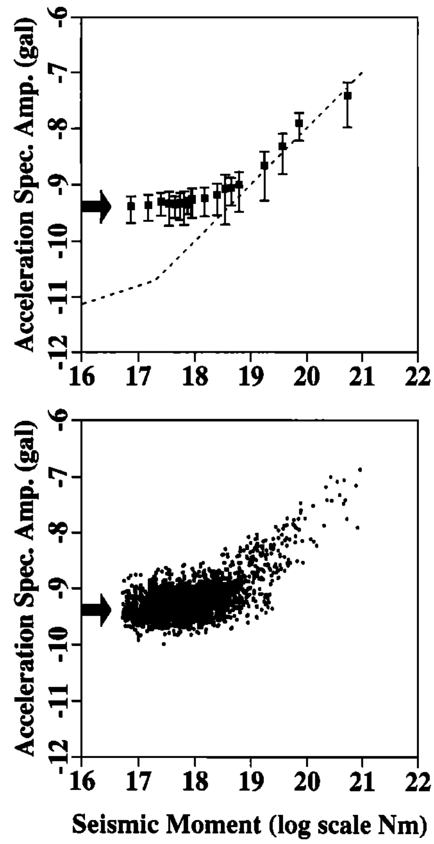

Figure 4b. Same as Figure 4a, except for CAN. The same flattening trend is seen in this figure.

are plotted at the bottom, and the median and variance (L1 norm) are shown in the top panel.

For days with large earthquakes (larger than about 10^{18} Nm), there is clearly a linear trend in Figures 4a and 4b, which show a log-log plot of moment versus A_{26}. The linear range spans from about 10^{18} to 10^{21} Nm. The dashed line in the figures is drawn as a reference and fits the trend in the data. The formula for this dashed line is given by

$$A_{26} = \frac{100(nGal)}{10^{21}} M_o \tag{4}$$

where M_o is moment in Nm and yields $A_{26} = 100$ nGal at $M_o = 10^{21}$ Nm. Because this mode is in the low-frequency band (about 3 mHz), the amplitude should be proportional to moment. Theoretically, this trend should continue to the small-moment range. We have applied corrections to this theoretical line for moments below 2×10^{17} Nm, because there is more than one earthquake per day on the average. This effect changes the gradient of the dashed line to a shallower gradient below this moment.

One of the most striking observational features in Figures 4a and 4b is the flattening trend of the amplitudes below 10^{18} Nm. It is not only constant for days with smaller earthquakes (down to 5×10^{16} Nm) but continues to the level derived from seismically quiet days. The arrows denote the average amplitude for seismically quiet days and are obtained from data in Figures 5a and 5b. Figures 5a and 5b show modal amplitude measurements of ${}_0S_{26}$ from seismically quiet days by solid and open circles; solid circles are average (acceleration) amplitudes for ${}_0S_{26}$ computed by averaging over ± 0.02 mHz about the (PREM) eigenfrequency of the mode. Open circles are background amplitudes, measured from the same spectra for the frequency range between the eigenfrequency of ${}_0S_{25}$ and that of ${}_0S_{26}$, again averaging over ± 0.02 mHz. Averages for solid circles and open circles are denoted by the solid and dashed lines, respectively, and they are shown by the arrows in Figures 4a and 4b.

These results suggest that, regardless of the size of earthquakes, as long as earthquakes are below 10^{18} Nm, this mode (${}_0S_{26}$) is excited at the observed level. Independent and equivalent evidence was reported by *Ekström* [1998], who gave a more precise threshold of magnitude 5.8. This feature, especially its constancy in amplitude, is not likely to be explained by the cumulative effect of small earthquakes. It seems more natural to interpret that some mechanism, other than earthquakes, is controlling the amplitudes of this mode; this mechanism must be an almost constant process in time, and only when large earthquakes occur (larger than 10^{18} Nm) is it overwhelmed by earthquake effects.

3.2. Cumulative Effect of Small Earthquakes

Figures 4a and 4b show earthquake effects by the dashed lines, but they are not cumulative effects. Cumulative effects must be evaluated by integrating from small earthquakes to a certain upper threshold in magnitude, with the weighting given by the number of earthquakes $n(M)$ as a function of magnitude M. Let us assume the form of the Gutenberg-Richter law for $n(M)$,

$$\log n(M) = a - bM. \tag{5}$$

We assume $b = 1.0$ and determine a by the fact that there is approximately one earthquake for $M > 8$ per year. Then we obtain

$$n(M) = \frac{\ln 10}{365} 10^{8-M} \tag{6}$$

for $n(M)$ per day. The amplitude-moment formula (4) can be converted to the amplitude-magnitude formula by using the moment (M_o in Nm)-magnitude (M) formula

$$\log_{10} M_o = 1.5M + 9.0. \tag{7}$$

The cumulative effect of small earthquakes should then be bounded by

$$\int_{-\infty}^{M_T} n(M)A(M)dM \approx 5.5 \times 10^{0.5M_T - 5}, \tag{8}$$

where the unit for amplitude is nGal and M_T is the maximum magnitude for the cumulative effects to be calculated. Note that this formula assumes perfectly constructive effects; if random contributions from each

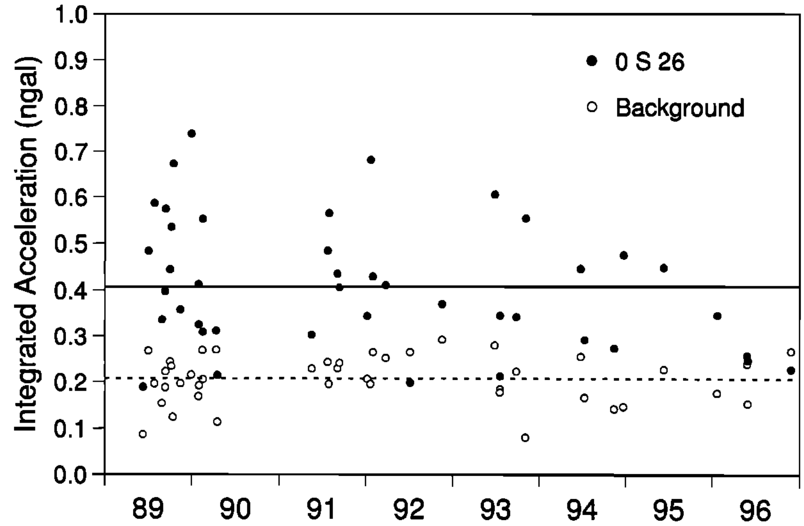

Figure 5a. Average accelerations of a spheroidal mode ${}_0S_{26}$ on seismically quiet days (solid circles) for KIP. Background noise was measured by integrating the frequency range between ${}_0S_{25}$ and ${}_0S_{26}$ (see text for details). This mode ${}_0S_{26}$ is above the noise level on most seismically quiet days, although there are a few exceptions.

earthquake are considered, $\sqrt{n(M)}$ rather than $n(M)$ should be used in the estimation. However, since we are interested in bounding the effects of small earthquakes, we use the above formula.

According to the formula (8), the cumulative effect of earthquakes up to magnitude 5 ($M_T = 5$) is 0.017 (nGal), while the observed amplitudes are about 0.2-0.4 nGal. Therefore the cumulative effect of small earthquakes is more than an order of magnitude too small to explain the observed amplitude of oscillations.

Combined with the constant amplitude observation for moment below about 10^{18} Nm, it is very unlikely that the cumulative effect of small earthquakes can explain the observed oscillations. Contradiction of this statement would require evidence for the violation of the Gutenberg-Richter frequency-magnitude relation for small earthquakes. However, the required b value change in the Gutenberg-Richter formula is quite large; for example, in order to explain the constant amplitude observation in section 3.1, there must be a reduction of b value from a typical value of 1 to about 0.3. This drastic change goes against most evidence accumulated by microearthquake studies, which typically report a b value of about 1 down to the negative magnitude range.

4. Seasonal Variation

Confirmation of seasonal variations in modal amplitudes is important because it constrains the range of possible excitation sources. This is particularly impor-

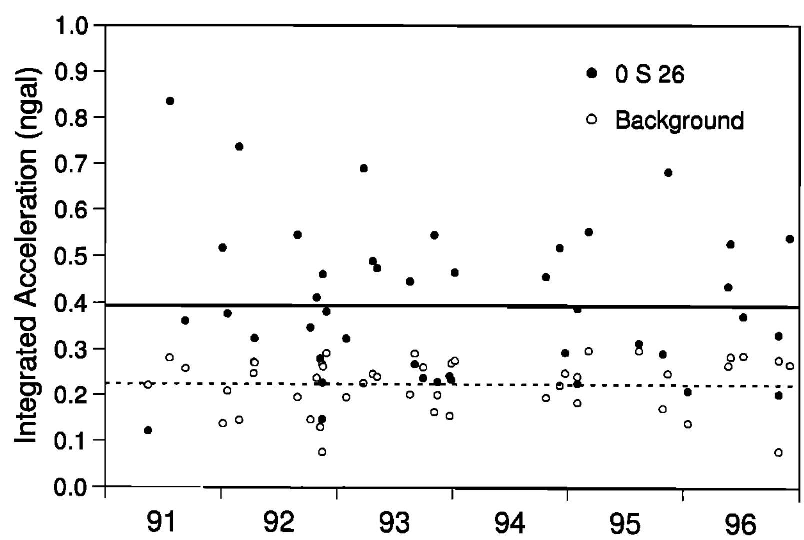

Figure 5b. Same as Figure 5a, except at CAN. There are more exceptions for this station, but, overall, ${}_0S_{26}$ seems to be excited on most days.

tant since most processes in the solid Earth do not show seasonal variations. Such an observation would suggest that the source is in the atmosphere or in the oceans. However, all of our initial efforts to detect such variations for a single mode failed, due probably to a low signal to noise ratio in the data. It became possible to detect seasonal variations only after we began to examine average modal amplitudes for modes between ${}_0S_{20}$ and ${}_0S_{40}$.

Since modal peaks such as those in Figure 1 have relatively constant amplitudes, a simple averaging procedure would not introduce bias toward any particular modes; thus we simply took an average of 21 spheroidal modes from ${}_0S_{20}$ to ${}_0S_{40}$. Technically, we proceeded as follows: Starting from the Fourier spectra computed for each day, we isolated each mode by using the eigenfrequencies from an Earth model PREM. We took spectral amplitudes within ± 0.01 mHz of each eigenfrequency of PREM and averaging 21 modes. Modal peaks are not exactly at the eigenfrequencies of PREM due to the fact that PREM is only an approximation to the average Earth model and also because the Earth's three-dimensional structure introduces eigenfrequency shifts for various geographic locations. Taking the average over the range ± 0.1 mHz seems to alleviate this problem. We then collected these averaged modal amplitudes for 21 modes from quiet days and examined their statistical behaviors; Figure 6a shows the results from nine stations, listed in the top nine rows of Table 1. A bell-shaped distribution of the data is found for all nine stations with a little skewness and some outliers.

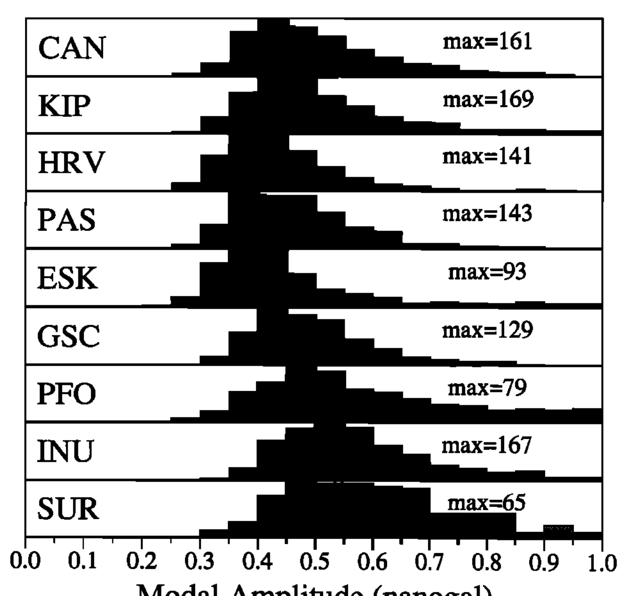

Figure 6a. Distribution of averaged modal amplitudes. The number of data within 0.5 ngal range is plotted. Analyses are performed for the data in the bell-shaped regions. In the case of SUR we set the upper limit as 0.7 nGal. Differences in the means are related to differences in background noise levels, but they are subtracted out in the analysis for the seasonal variations.

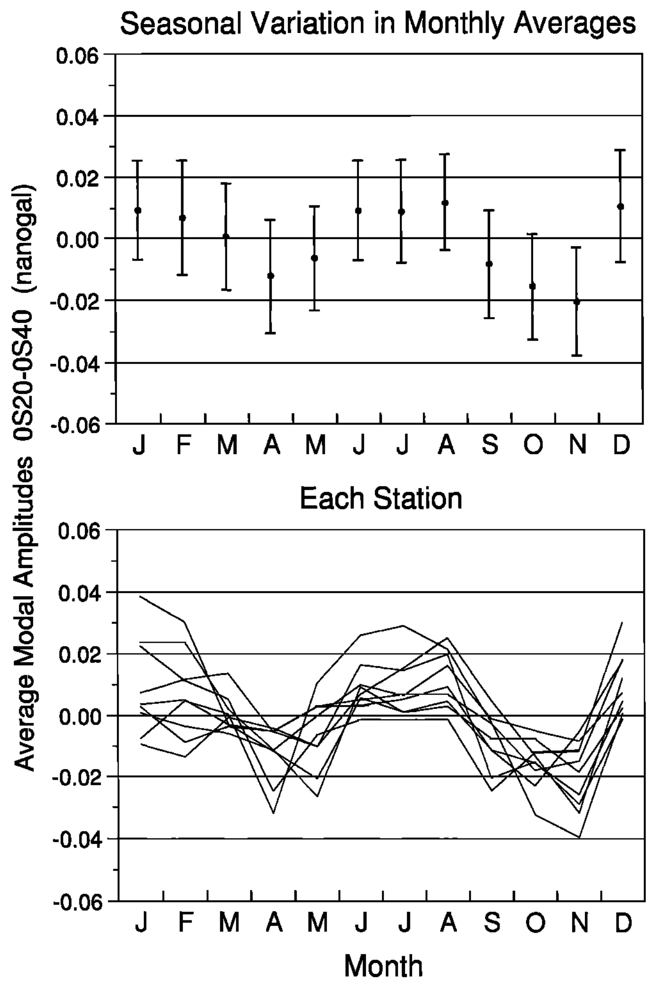

Figure 6b. Seasonal variations in averaged modal amplitudes. Average modal amplitudes for modes between ${}_0S_{20}$ and ${}_0S_{40}$ are plotted. The bottom panel shows the results from nine stations, given in the top nine rows of Table 1. When the poles are toward the Sun (summer and winter), amplitudes are higher.

It is generally easy to identify the extent of bell-shaped regions; the only exception may be SUR, for which we assigned the upper limit of 0.7 nGal (a change to 0.75 nGal does not alter the result very much). We focused on data from bell-shaped regions, binned the data according to months, subtracted the average for each station, and applied statistical analysis. Differences in the mean values among nine stations may result from differences in the background noise level (dashed lines in Figure 1), but they are subtracted out in the analysis. We examined variations about the means for this paper.

Figure 6b shows the monthly averages of data. In the top panel, monthly averages and their standard errors from all stations are given by circles and error bars. Error bars represent one standard error, suggesting that these variations are resolved but perhaps marginally. In the bottom panel, lines shown for each station in monthly averages demonstrate that all stations contain very similar seasonal variation patterns; high amplitudes are observed in June-July-August and December-January-February, and low amplitudes are observed in March-April-May and September-October-November. Peak-to-peak variations of these amplitudes are 5-10the average modal amplitudes, approximately agreeing with seasonal pressure variations in barometer data. While there are some differences from station to station, this seasonal variation pattern seems to hold for seven stations in the Northern Hemisphere as well as two stations in the Southern Hemisphere. This result suggests that when either the north pole or the south pole is pointing toward the Sun, these oscillations are excited at higher amplitudes. The real cause of this pattern may be the occurrence of winter in some parts of the world, either in the Northern Hemisphere or in the Southern Hemisphere, since average atmospheric pressure variation in each hemisphere is known to have a maximum in winter and a minimum in summer [*Peixoto and Oort*, 1992].

5. Atmospheric Excitation

In this section we examine the atmospheric excitation hypothesis, using the estimated pressure variations as the source of excitation. We present the formula, discuss the sensitivity of some parameters to the acceleration amplitudes, and compare the theoretical estimates to the data. The main conclusion is that atmospheric pressure variations can excite normal modes to the observed level.

5.1. Background and Basic Formula

In order to excite normal modes at frequencies of a few millihertz by the atmosphere, the atmosphere must supply energy in this frequency band. As we discussed above with Figures 2a and 2b, atmospheric motion in this frequency band indicates turbulent motion. Therefore the source of excitation must be a stochastic force, and the theory must take into account such a feature of the source. *Tanimoto* [1999] considered a problem of normal mode excitation by a stochastic source, which we basically follow in this paper. Its main conclusion can be summarized as follows. Let $u_i(t)$ be the displacement; then $u_i(t)$ can be written as a summation of normal modes as

$$u_i(t) = \sum_n a_n(t) u_i^{(n)}, \qquad (9)$$

where $a_n(t)$ is the excitation coefficient for the nth normal mode and $u_i^{(n)}$ is the eigenfunction. If a global stochastic force is applied at the surface of the Earth, the excitation coefficient can be written by

$$\begin{aligned} < | \quad a_n \quad |^2 >= \frac{R^4}{I_n^2} \int_S d\Omega' \int_S d\Omega'' \int_{-\infty}^{t} dt' \int_{-\infty}^{t} dt'' \\ \times u_i^{(n)}(\Omega') u_i^{(n)}(\Omega'') \exp\{-\frac{\omega_n(2t - t' - t'')}{2Q_n}\} \\ \times \frac{\sin \omega_n(t-t') \sin \omega_n(t-t'')}{\omega_n^2} \\ \times < f(t', \Omega') f(t'', \Omega'') >, \end{aligned} \qquad (10)$$

where R is the radius of the Earth, I_n is the normalization of an eigenfunction, Ω' and Ω'' are the spatial integration variables on the surface of the Earth, and t' and t'' are the time integration variables. Q_n is the attenuation parameter for the nth mode, ω_n is its eigenfrequency, and the force (pressure) correlation $< f(t', V'); f(t'', V'') >$ is the source of excitation. There are two spatial variables and two temporal variables because spatial correlation and temporal correlation are the keys to this problem. The existence of this temporal correlation term distinguishes our formulation from that in the work by *Kobayashi and Nishida* [1998], although it is not the only difference.

In the most general case the force term has contributions from various wavelength components and can be written [e.g., *Goldreich and Keeley*, 1977]

$$\begin{aligned} < f(t', \Omega') f(t'', \Omega'') >= \\ \int_0^{H_s} \frac{d\lambda}{\lambda} P_\lambda^2(\Omega', \Omega'') G_\lambda(t', t'') H_\lambda(\Omega', \Omega''), \end{aligned} \qquad (11)$$

where the integration with respect to wavelength is performed from 0 to the scale height of the atmosphere, H_s, for which we use $H_s = 8.7$ km in this paper. The exact upper limit does not affect the final results because the integrand decreases to a small value well before this upper limit is reached, at least for the range of modes of our interest. P_λ^2 is the power and is the square of pressure variations, $G_\lambda(t', t'')$ is the temporal correlation function, and $H_\lambda(\Omega', \Omega'')$ is the spatial correlation function; all are functions of wavelength λ. The relationship for pressure variations, obtained in section 2, is used for P_λ; the Kolmogorov scaling law provides the wavelength dependence of the integrand in the above formula and has the following features [e.g., *Landau and Lifshitz*, 1987; *Frisch*, 1995; *Tennekes and Lumley*, 1972]:

$$P_\lambda = P_H (\frac{\lambda}{H_s})^{2/3}, \qquad (12)$$

where P_H is the pressure variation at the longest wavelength, which is equal to the scale height H_s. The characteristic time for various sizes of turbulent eddies is given by $\tau_\lambda = 2\lambda / v_\lambda$ for wavelength λ. The longest characteristic time is for the wavelength equal to the scale height H_s and is given by $\tau_H = 2H_s / v_{H_s}$ (for this period, we write τ_H instead of τ_{H_s}). Velocity at wavelengths λ and velocity at H are related by $v_\lambda / v_{H_s} = (\lambda / H_s)^{1/3}$. Using the ratio $\tau_\lambda / \tau_H = (\lambda / H_s)^{2/3}$, the above pressure relation can be converted to

$$P_\lambda = P_H \frac{\tau_\lambda}{\tau_H}, \qquad (13)$$

which then becomes a relation in the frequency domain (period). There is thus a one-to-one correspondence between the wavelength of an eddy and its frequency, although it is nonlinear.

For the time correlation function, we assume the form

$$G(t', t'') = \exp\{-\frac{(t' - t'')^2}{(k_\tau \tau / 5)^2}\}, \qquad (14)$$

where we dropped λ from τ and maintain this convention hereafter. This functional form has been used in heleoseismology for the last 20 years [e.g., *Goldreich and Keeley*, 1977; markcite*Balmforth*, 1992] for the stochastic excitation of Sun's normal modes by turbulent convection. Division by 5 is introduced here, because two sinusoids with the same periodicity τ lose correlation if they are shifted by $\tau/4$. At a time shift of $\tau/5$, the correlation becomes about $1/e$; since we assume the exponential form, we adopt this factor. However, because there are obviously some uncertainties in this parameter, we introduce k_τ, which is a constant of order unity. We will examine the sensitivity of this parameter on the theoretical estimates in the next section.

For the spatial correlation function, we simply assume $H_\lambda = 1$ if the distance between two points, Ω' and Ω'', is less than the wavelength λ, and $H_\lambda = 0$ otherwise. As the subscript indicates, it changes with wavelength. Mathematically, we express this as

$$\int_S d\Omega'' H_\lambda(\Omega', |\Omega' - \Omega''|) u_i^{(n)}(\Omega'') = \pi\lambda^2 k_\Omega u_i^{(n)}(\Omega'). \tag{15}$$

Again we introduced a factor of order unity, k_Ω, and examine its sensitivity in the final results.

Under these assumptions we can evaluate the integrals in (10) (see the appendix). Since the data are vertical component seismograms and are given in units of acceleration, the formula for the vertical acceleration is given here:

$$\begin{aligned} A_n &= \omega^2 \sqrt{< |a_n|^2 >} U_n(R) \\ &= 1292 \frac{\sqrt{Q_n} R H_s P_H}{(\omega_n \tau_H)^{5/2} M_n} \sqrt{\frac{k_\Omega}{k_\tau^5}} F\left(\frac{\omega^2 \tau_H^2 k_\tau^2}{100}\right), \end{aligned} \tag{16}$$

where M_n is the modal mass and is defined in this paper by

$$\frac{1}{M_n} = \frac{\sqrt{U_n(R)^2 + l(l+1)V_n(R)^2} U_n(R)}{\int_E \rho_s \{U_n(r)^2 + l(l+1)V_n(r)^2\} r^2 dr}. \tag{17}$$

U_n and V_n are the vertical and horizontal eigenfunctions of a spheroidal mode [e.g., *Aki and Richards* 1980].

The function $F(x)$ in (16) is very close to 1 when x is large but deviates from it when x is small (see equation (24) in the appendix). Generally, if the frequency is close to $1/\tau_H$, it deviates from 1, but quickly reaches 1 for high-frequency modes.

5.2. Sensitivity

In the formula for acceleration amplitude (16), there are basically three uncertain parameters; the first is the low-frequency cutoff, $1/\tau_H$, that corresponds to the frequency of the largest scale of the eddy. The other two are k_τ and k_Ω, two constants introduced in consideration of the temporal correlation and the spatial correlation. Among these three parameters, the sensitivity of k_Ω on the acceleration is relatively easy to predict, since acceleration is simply proportional to $\sqrt{k_\Omega}$. The dependence of the other parameters is harder to understand intuitively.

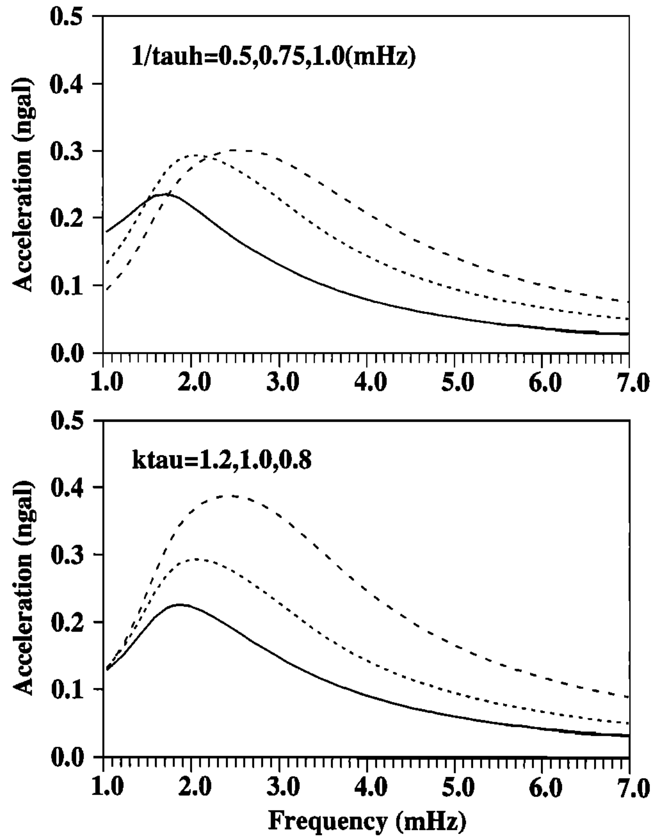

Figure 7. Sensitivity analyses for (top) τ_H and (bottom) k_τ.

Figure 7 shows the sensitivity of τ_H (top) and of k_τ (bottom) to the acceleration estimate given by (16). In the discussion of barometer data, we showed that it is difficult to determine at which frequency the energy-containing eddy exists ($1/\tau_H$). Figure 2a seems to indicate that it starts near 1 mHz but with large uncertainty. In the top panel of Figure 7, in order to examine how the choice of this parameter affects modal amplitudes, we show three different cases of $1/\tau_H$: 0.5 mHz (solid line), 0.75 mHz (short-dashed line), and 1 mHz (long-dashed line). Both k_τ and k_Ω are fixed at 1.0 ($k_\tau = k_\Omega = 1.0$). Pressure variations at these frequencies are computed by $P(f) = 0.32/f$. This figure basically shows two features; one is that as $1/\tau_H$ is increased, the peaks move toward higher frequencies. The other feature is that the change in amplitude is less than 30-40and is much smaller than the effects of k_τ, shown in the bottom panel.

The bottom panel shows the results when k_τ was varied as $k_\tau = 1.2$, 1.0, and 0.8, while $1/\tau_H$ was fixed at 0.75 mHz and k_Ω at 1. In the acceleration formula, k_τ appears in the coefficient as $k_\tau^{-5/2}$, in addition to the argument of the function $F()$. The figure indicates that a decrease of k_τ from 1.2 to 0.8 increases the amplitudes by about a factor of 2, while the locations of peaks move toward higher frequencies.

It is clear that these parameters introduce some uncertainties into the estimates of acceleration amplitudes.

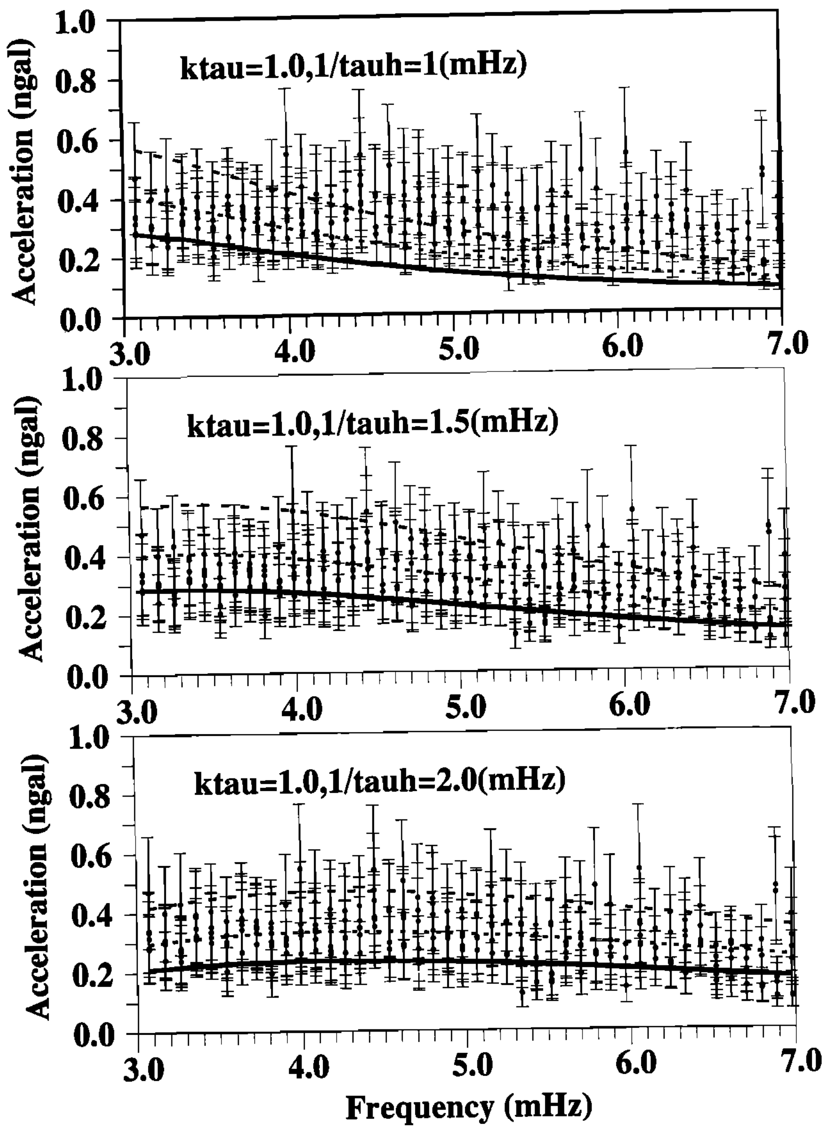

Figure 8. Three different cases of k_τ and τ_H are compared with modal amplitude data (solid circles). In each panel, three curves correspond to different values of k_Ω (see text). The best fit is achieved by the bottom panel, which has the energy-containing eddy at frequency 2 mHz. Overall, stochastic atmospheric pressure fluctuation can generate 0.2-0.4 nGal of modal amplitudes and supports the atmospheric excitation hypothesis.

Variations of a factor of 2-3 may be introduced into the acceleration estimates within the reasonable range of these parameters. Therefore we conclude that this theory does not have precise predictive capability. Rather, it basically provides order of magnitude estimates for excited modal amplitudes. Considering the constraints (pressure range) provided by barometer data, however, it would be hard to change the estimates by an order of magnitude.

5.3. Comparison Between Theory and Data

Since the sensitivity analysis shows unavoidable uncertainties of our estimates by a factor of 2-3, we do not attempt to exactly fit spectral amplitude data by theory. Instead, we present a few different cases of typical parameter ranges and discuss comparisons between theory and observation. In evaluating the formula (16), except for the three parameters we vary, we fixed the scale height of the atmosphere $H_s = 8.7$ km, the Earth's radius $R = 6371$ km, pressure variations P_H computed by $P = 0.32/f$, and modal parameters (eigenfrequency ω_n, its modal mass M_n, and its attenuation parameter Q_n) to those of the standard Earth model PREM.

Figure 8 shows three plots, each of which contains three different cases of theoretical predictions. From top to bottom, k_τ is held at 1.0 ($k_\tau = 1.0$) and $1/\tau_H$ is varied as $1/\tau_H = 1.0$ mHz (top), 1.5 mHz (middle), and 2.0 mHz (bottom). In each panel, three cases of k_Ω are given by a solid line, a short-dashed line, and a long-dashed line, the values being $k_\Omega = 1$, 2, and 4. In all

Table 2. Modal Amplitudes at Six Stations

Mode	CAN	KIP	PAS	HRV	PFO	SUR
0 S 20	0.29	0.27	0.31	0.35	0.31	0.25
0 S 21	0.18	0.24	0.23	0.30	0.29	0.39
0 S 22	0.34	0.32	0.28	0.34	0.29	0.47
0 S 23	0.40	0.24	0.30	0.30	0.31	0.31
0 S 24	0.26	0.24	0.28	0.28	0.27	0.43
0 S 25	0.35	0.39	0.31	0.32	0.39	0.39
0 S 26	0.33	0.41	0.35	0.30	0.08	0.34
0 S 27	0.37	0.29	0.30	0.33	0.20	0.23
0 S 28	0.37	0.38	0.36	0.27	0.41	0.34
0 S 29	0.33	0.36	0.35	0.34	0.29	0.37
0 S 30	0.36	0.35	0.20	0.29	0.30	0.33
0 S 31	0.26	0.31	0.31	0.31	0.42	0.29
0 S 32	0.36	0.41	0.32	0.33	0.54	0.26
0 S 33	0.31	0.33	0.34	0.35	0.43	0.27
0 S 34	0.27	0.35	0.28	0.26	0.39	0.41
0 S 35	0.23	0.40	0.31	0.31	0.26	0.37
0 S 36	0.32	0.35	0.34	0.37	0.26	0.42
0 S 37	0.38	0.47	0.37	0.35	0.54	0.44
0 S 38	0.27	0.40	0.41	0.29	0.40	0.41
0 S 39	0.39	0.29	0.38	0.28	0.50	0.37
0 S 40	0.22	0.44	0.36	0.27	0.23	0.40
0 S 41	0.33	0.38	0.42	0.27	0.30	0.44
0 S 42	0.34	0.32	0.31	0.23	0.30	0.40
0 S 43	0.37	0.28	0.27	0.23	0.40	0.31
0 S 44	0.31	0.39	0.30	0.26	0.38	0.30
0 S 45	0.35	0.29	0.34	0.25	0.37	0.48
0 S 46	0.25	0.36	0.35	0.25	0.43	0.36
0 S 47	0.23	0.35	0.40	0.12	0.26	0.35
0 S 48	0.35	0.24	0.16	0.22	0.21	0.32
0 S 49	0.18	0.34	0.15	0.16	0.18	0.35
0 S 50	0.36	0.23	0.29	0.28	0.41	0.25
0 S 51	0.18	0.40	0.27	0.28	0.32	0.30
0 S 52	0.25	0.48	0.24	0.24	0.26	0.21
0 S 53	0.27	0.41	0.29	0.21	0.27	0.24
0 S 54	0.00	0.05	0.23	0.14	0.05	0.28

Data are in nanoGals.

cases the smaller the k_Ω, the smaller the acceleration amplitude. The observed modal amplitudes from six stations (Table 2) are plotted by circles with error bars.

The match between theory and data is generally good in these plots, in particular, the bottom panel. They demonstrate that atmospheric pressure change at the surface is capable of exciting solid Earth normal modes up to the level of about 0.2-0.4 (nGal). They also suggest that in order to fit the overall frequency trend in the data, the frequency of energy-containing eddies ($1/\tau_H$) should be close to 2 mHz rather than 0.5 or 1 mHz.

We thus conclude that the stochastic atmospheric excitation theory can explain amplitudes of continuously excited normal modes. Even though the observed atmospheric pressures are incoherent at a short distance of 150 km (and probably at an even shorter distance about 20-30 km), they are sufficient to excite the oscillations of the Earth through the stochastic excitation process.

6. Discussion

We mainly discuss two subjects here. The first will deal with possible future observations which can reduce uncertainties in our theory. The second deals with the differences between our theory and the theory presented by *Kobayashi and Nishida* [1998].

6.1. Future Observation

While the theory presented in this paper can generally explain modal amplitudes, it does contain a few important assumptions which should be tested by data in the future. These are mainly associated with the three parameters we introduced in the above discussion, τ_H, k_τ, and k_Ω, for which we have very few observational constraints.

The most critical parameter among them is clearly k_τ because of the $k_\tau^{-5/2}$ dependence in the final formula (16). It is certainly desirable for this parameter (on temporal correlation) to be constrained observationally by barometer data. However, this is hard to do at present, because our theory requires the temporal correlation function as a function of wavelength. The expected correlation disappears at a distance of about 10 km, which is comparable to the scale height of the atmosphere. This suggests that we need to install barometers at an interval of 2-3 km or less in order to constrain this parameter. At present, all available barometer data (to us) are separated by about 100 km and do not provide useful information on this parameter.

A similar argument applies to spatial correlation (or the parameter k_Ω), although this is less sensitive to the final result because of $\sqrt{k_\Omega}$ dependence on amplitude. It is obvious that if we want to better constrain those parameters and sharpen our theoretical estimates, we would need a much denser array of barometer data.

6.2. Comparison With Previous Study

Recently, *Kobayashi and Nishida* [1998] presented a similar argument on the atmospheric excitation of normal modes. Our main conclusion does not differ from theirs, although our approaches and the final formulas differ and thus necessitate making some comments.

In terms of the large-scale picture, the questions we attempted to solve were actually (slightly) different. This paper and that of *Tanimoto* [1999] sought the solution of expected normal mode excitation when stochastic force acts on the surface of the Earth. *Kobayashi and Nishida* [1998] solved for the surface acceleration formula when a steady state is assumed for the balance of energy between the energy from the atmosphere to a mode and the energy dissipated through oscillations. Such a steady state is not assumed in our approach, although the results led toward that direction because of the statistical behavior of atmospheric pressure. Because of this difference in the questions, the two approaches can obviously lead to different results (formulas). In the following we list some of our observations on the differences and our thoughts on them.

First of all, *Kobayashi and Nishida* [1998] theory does not contain the temporal correlation term. It appears to us that temporal correlation is an important property in atmospheric turbulence (or pressure variations). Depending on the temporal correlation function, amplitudes of excited modes would differ by almost an order of magnitude. Their theory is equivalent to assuming it to be one for all wavelengths, while our theory uses a smaller number (described by the exponential function used for $G_\lambda(t', t'')$). This term should also introduce frequency dependence of amplitudes.

Second, *Kobayashi and Nishida* [1998] started with a formula that shows the balance of energy between work done by the atmosphere on a particular mode and the kinetic energy of the same mode. In view of the strain energy and the gravitational energy, this may not be justified; although this difference may amount to only a small factor. They also used surface particle velocity in expressing the kinetic energy of a mode, which should also introduce a small discrepancy because modal amplitudes decrease with depth.

Third, our formula (16) shows that acceleration amplitude is proportional to $\sqrt{Q}$, whereas their theory shows amplitude is proportional to Q. Since modal Q values are about 200-300, this would lead to a significant difference for modal amplitudes. This difference also originates in the basic assumptions of our approaches. In our theory it seems inescapable that the formula will have $\sqrt{Q}$ dependence, because a stochastic theory involves computation of an ensemble which would always lead to a term proportional to Q for a decaying sinusoid; modal amplitude for acceleration (and for velocity and displacement) is proportional to its square root and thus a $\sqrt{Q}$ term must emerge from such an analysis. Q dependence in the work by *Kobayashi and Nishida* [1998] originates in the assumption that in order to have the steady state, energy input for a mode must be proportional to $\omega E/Q$, where E is the kinetic energy of a mode. Their result directly follows from this assumption.

Fourth, the pressure value that *Kobayashi and Nishida* [1998] used for the Earth (17 Pa at $1/\tau_H$, their Table 1) is more than an order of magnitude larger than the observed pressures from barometer data. Correction on this point will make theoretical estimates based on their formula smaller than observation by an order of magnitude.

Those differences indicate that the two approaches (theories) are quite different. While both reached qualitatively the same conclusion, that the atmosphere can excite normal modes of the Earth at the observed level, this may be more of a coincidence.

7. Conclusions

The main points of this paper can be summarized as follows:

1. Even for days without effects from earthquakes larger than the moment 10^{18} Nm, fundamental spheroidal modes between 3 and 7 mHz are observed almost every day and have acceleration amplitudes of about 0.2-0.4 nGal. This requires an equivalent earthquake of magnitude 6.0 every day.

2. The cumulative effect of small earthquakes is simply too small to explain the observed amplitudes. This argument fails if large deviation from the Gutenberg-Richter magnitude-frequency law occurs for small earthquakes, but such a violation is not very likely. Also the cumulative effect cannot explain the constancy of observed modal amplitudes below the moment about 10^{18} Nm; in principle, if the b value is as low as 0.3, this could be explained, but such a low value is inconsistent with previous microearthquake studies.

3. Seasonal variation is detected in average modal amplitude data for 21 spheroidal modes between ${}_0S_{20}$ and ${}_0S_{40}$. High amplitudes are seen in June-August and in December-February when either the north pole or the south pole is pointing toward the Sun. The critical cause may be the occurrence of winter in some parts of the world, since atmospheric pressure (hemispherical average) is known to have a maximum in winter and a minimum in summer. Because of the detection of this variation, the excitation source is not likely to be in the solid Earth.

4. The observed modal amplitudes can be quantitatively matched by the stochastic normal mode theory, using the observed atmospheric pressure variation as input. Even though the atmospheric surface pressure is spatially incoherent, globally applied random pressure fluctuation is sufficient to generate normal modes to the observed level through the stochastic excitation process.

Appendix: Evaluation of Integrals

In the analytical evaluation of the integrals, the most difficult part is in evaluating the following integral K:

$$K \equiv \int_{-\infty}^{t} dt' \int_{-\infty}^{t} dt'' e^{-\frac{\omega}{2Q}(2t-t'-t'')} \times \frac{\sin\omega(t-t')\sin\omega(t-t'')}{\omega^2} e^{-\frac{(t'-t'')^2}{\tau^2}}. \quad (18)$$

This integral can be evaluated by changing the integration variables from t' and t'' to t_+ and t_- defined by $t_+ = (t'+t'')/2$ and $t_- = (t'-t'')/2$. Then it becomes

$$K = \frac{2}{\omega^2}\int_0^{\infty} dt_- \int_{-\infty}^{t-t_-} dt_+ e^{-\frac{\omega}{Q}(t-t_+)} \times\{\cos 2\omega t_- - \cos 2\omega(t-t_+)\} e^{-\frac{4t_-^2}{\tau^2}}. \quad (19)$$

Complete analytical evaluation is straightforward from this formula. However, if we can assume $Q \gg 1$, which is true for Earth's fundamental spheroidal modes (typically 200-300), the expression becomes much simpler. Keeping only the terms with $O(Q)$, we obtain

$$K = \sqrt{\pi}\frac{Q\tau}{\omega^3} e^{-\frac{\omega^2\tau^2}{4}}. \quad (20)$$

This formula will allow us to remove two integrations with respect to t' and t'' in (10). Combined with the assumption on the spatial integration (15), we obtain

$$< |a_n|^2 > = \frac{\pi^{3/2} Q_n R^2 k_\tau k_\Omega}{5\omega_n^3 I_n^2} \int_S d\Omega \{u_i^{(n)}(R,\Omega)\}^2 \times \int_0^{H_s} d\lambda\, \lambda\, \tau\, P_\lambda^2\, e^{-\frac{\omega_n^2 k_\tau^2 \tau^2}{100}}. \quad (21)$$

The integration with respect to Ω simply produces $U_n^2 + l(l+1)V_n^2$. The integration with respect to λ is converted to one with respect to τ by using the relation

$$\frac{\tau}{\tau_H} = (\frac{\lambda}{H})^{2/3}. \quad (22)$$

This integration with respect to τ can be analytically evaluated by using

$$\int_0^{\tau_H} d\tau \tau^5 e^{-\alpha\tau^2} = \frac{1}{\alpha^3}(1 - e^{-\alpha\tau_H^2} - \alpha\tau_H^2 e^{-\alpha\tau_H^2} - \frac{\alpha^2\tau_H^4}{2} e^{-\alpha\tau_H^2}). \quad (23)$$

By defining the function $F()$ by

$$F(x) = \sqrt{1 - e^{-x} - xe^{-x} - \frac{x^2}{2}e^{-x}}, \quad (24)$$

we obtain the expression (16) after some lengthy but straightforward algebra.

In the above derivation it may appear that setting the upper integration limit as H_s in (21) is rather arbitrary and is not necessarily justified. It turns out, however, that the final result is not sensitive to this upper limit. This is because the integrand contains an exponentially decaying term for long wavelengths and decreases to a very small number well before $\lambda = H_s$ is reached. This can also be confirmed in the transformed integration with respect to τ in (23). For modes with eigenfrequencies above 2 mHz, the exponentially decaying term $\exp(-\alpha\tau_H^2)$ becomes so small that this integral is well approximated by the first term only ($1/\alpha^3$ on the right-hand side); this is equivalent to saying that the upper limit in (21) is insensitive to the final result or it is sufficiently large. This statement does not apply to low-frequency modes below 1 mHz, but the observed continuous oscillations are all above 2 mHz.

Acknowledgments. We thank the Associate Editor and the referees, Tony Dahlen and Walter Zürn, for valuable comments. This work was supported by the Caltech President's Fund, the California Space Institute and NASA. Contribution ICS0341-91EQ, Institute of Crustal Studies, University of California, Santa Barbara.

References

Agnew, D. C., J. Berger, W. E. Farrell, J. F. Gilbert, G. Masters and D. Miller, Project IDA: A decade in review, *Eos, Trans. AGU*, *67*, 203-212, 1986.

Aki, K. and P. G. Richards, *Quantitative Seismology: Theory and Methods*, W. H. Freeman, New York, 1980.

Balmforth, N. J., Solar pulsational stability III, Acoustical excitation by turbulent convection, *Mon. Not. R. Astrono. Soc.*, *255*, 639-649, 1992.

Beroza, G., and T. Jordan, Searching for slow and silent earthquakes using free oscillations, *J. Geophys. Res.*, *95*, 2485-2510, 1990.

Crossley, D. J., O. G. Jensen, and J. Hinderer, Effective barometric admittance and gravity residuals, *Phys. Earth Planet. Inter.*, *90*, 221-241, 1995.

Dahlen, F. A., The normal modes of a rotating, elliptical Earth, *Geophys. J. R. Astron. Soc.*, *16*, 329-367, 1968.

Dziewonski, A. M., and D. L. Anderson, Preliminary reference Earth model, *Phys. Earth Planet. Inter.*, *25*, 297-356, 1981.

Dziewonski, A. M., and J. H. Woodhouse, Studies of the seismic source using normal mode theory, *Proc. Enrico Fermi Sch. Phys.*, *85*, 45-137, 1983.

Ekström, G., Time domain analysis of Earth's background seismic radiation (abstract), *Eos Trans. AGU*, *79*, Fall Meet. Suppl., F628-F629, 1998.

Frisch, U., *Turbulence*, Cambridge Univ. Press, New York, 1995.

Garratt, J. R., *The atmospheric boundary layer*, Cambridge Univ. Press, New York, 1992.

Gilbert, F., Excitation of normal modes of the Earth by earthquake sources, *Geophys. J. R. Astron. Soc.*, *22*, 223-226, 1971.

Goldreich, P., and D. A. Keeley, Solar seismology, II, The stochastic excitation of the solar p-modes by turbulent convection, *Astrophys. J.*, *212*, 243-251, 1977.

Kaimal, J. C. and J. J. Finnigan, *Atmospheric Boundary Layer Flows*, Oxford Univ. Press, New York, 1994.

Kobayashi, N., and K. Nishida., Continuous excitation of planetary free oscillations by atmospheric disturbances, *Nature*, *395*, 357-360, 1998.

Landau, L. D., and E. M. Lifshitz, *Fluid Mechanics, Course Theor. phys.*, vol. 6, 2nd ed., Pergamon Press, New York, 1987.

Lognonné, P., E. Clevede, and H. Kanamori, Computation of seismograms and atmospheric oscillations by normal mode summation for a spherical Earth model with realistic atmosphere, *Geophys. J. Int.*, *135*, 388-406, 1998.

Müller, T., and W. Zürn, Observation of gravity changes during the passage of cold fronts, *J. Geophys.*, *53*, 155-162, 1983.

Nawa, K., N. Suda, Y. Fukao, T. Sato, Y. Aoyama, and K. Shibuya, Incessant excitation of the Earth's free oscillations, *Earth Planets Space*, *50*, 3-8, 1998.

Panofsky, H. A., and J. A. Dutton, *Atmospheric Turbulence: Models and Methods for Engineering Applications*, John Wiley, New York, 1984.

Peixoto, J., and A. H. Oort, *Physics of Climate*, Springer-Verlag, New York, 1992.

Roult, G., and J. P. Montagner, The Geoscope program, *Ann. Geofis.*, *37*, 1054-1059, 1994.

Saito, M., Excitation of free oscillations and surface waves by a point source in a vertically heterogeneous Earth, *J. Geophys. Res.*, *72*, 5963-5984, 1967.

Suda, N., K. Nawa, and Y. Fukao. Earth's background free oscillations, *Science*, *279*, 2089-2091, 1998.

Tanimoto, T., Excitation of normal modes by atmospheric turbulence: Source of long period noise, *Geophys. J. Int.*, *136*, 395-402, 1999.

Tanimoto, T., J. Um, K. Nishida, and N. Kobayashi, Earth's continuous oscillations observed on seismically quiet days, *Geophys. Res. Lett.*, *25*, 1553-1556, 1998.

Tennekes, H., and J. L. Lumley, *A First Course in Turbulence*, MIT Press, Cambridge, Mass., 1972.

Warburton, R. J., and J. M. Goodkind, The influence of barometric-pressure variations on gravity, *Geophys. J. R. Astron. Soc.*, *48*, 281-292, 1977.

Warburton, R. J., and J. M. Goodkind, Detailed gravity-tide spectrum between one and four cycles per day, *Geophys. J. R. Astron. Soc.*, *52*, 117-136, 1978.

Watada, S., Near-source acoustical coupling between the atmosphere and the solid Earth during volcanic eruptions, Ph.D. thesis, Calif. Inst. of Technol., Pasadena, 1995.

Zürn, W., and R. Widmer, On noise reduction in vertical seismic records below 2 mHz using local barometric pressure, *Geophys. Res. Lett.*, *22*, 3537-3540, 1995.

T. Tanimoto, Department of Geological Sciences, University of California, Santa Barbara, California 93106. (e-mail: toshiro@magic.geol.ucsb.edu)

J. Um, Institute of Crustal Studies, University of California, Santa Barbara, CA93106. (email: junho@mantle.geol.ucsb.edu)

(Received January 7, 1999; revised July 5, 1999; accepted July 14, 1999.)